

$$D = \{\omega_c [e^{-Fu(0)} - (1/2\omega_c F^2)(e^{-Fu(0)} - e^{-Fu(\Delta)})]\}^{-1}, \quad (A16)$$

$$S(\varphi, \varphi') = s(\varphi)s(\varphi'),$$

$$u(\varphi) = \int s(\varphi) d\varphi,$$

and

$$F = (1/\omega_c)[u(\Delta) - u(0)].$$

In the simplest case, where $s(\varphi) = C^{1/2}$, $0 \leq \varphi \leq \Delta$, we find using (A11) that

$$P = -\frac{1}{2} \left(1 + \frac{e^{-1/\omega_c T} - \frac{1}{2}\omega_c T(1 - e^{-1/\omega_c T})}{1 - \frac{1}{2}\omega_c T(1 - e^{-1/\omega_c T})} \right), \quad (A17)$$

$$Q = 1 - P,$$

in agreement with Eq. (29).

The fact that $P < \frac{1}{2}$ as $\omega_c T \rightarrow 0$ can be explained as follows. In the case where $C \rightarrow \infty$ (i.e., $\omega_c T \rightarrow 0$) the particle is uniformly scattered over a region of width Δ in channel B as soon as it enters the scattering region at $t=0$. During the next increment of time a fraction of this uniform probability density flows out of channel B , the remainder of the density being uniformly scattered back into channel A . During the next increment of time the same process described above occurs in channel A ; however, the amount of probability density that flows out of channel A during this second increment of time is less than that which originally flowed out of channel B an instant before. This same periodic process continues as $t \rightarrow \infty$. If we now subtract the probability density emerging in channel A from that emerging in channel B in a pairwise fashion it is obvious that $Q - P > 0$, and thus that $P < \frac{1}{2}$ as $\omega_c T \rightarrow 0$.

Electron-Hole Recombination in Bismuth*

A. A. LOPEZ

IBM Watson Laboratory, Columbia University, New York, New York 10025

and

Swiss Federal Polytechnic Institute (ETH), Zurich, Switzerland

(Received 29 May 1968)

We have measured the electron-hole recombination time τ_R in bismuth at temperatures from 2 to 50°K for two single-crystal samples with residual resistivity ratios, $\rho_{300^\circ\text{K}}/\rho_{4.2^\circ\text{K}}$, of 260 and 560. Above $\sim 6^\circ\text{K}$, the value of τ_R is the same for both samples and decreases rapidly as the temperature increases from $\sim 10^{-8}$ sec at 6°K. We postulate a model in which the absorption or emission of a single phonon provides for momentum conservation in the recombination of electrons and holes. The data above $\sim 6^\circ\text{K}$ can be fitted with two phonons, one of energy $(43 \pm 4)^\circ\text{K}$, the other $(130 \pm 15)^\circ\text{K}$. We have determined, by group-theoretical methods, the selection rules for the phonons involved, and have shown our data to be consistent with them. At lower temperatures, τ_R becomes a function of sample purity. Below $\sim 3^\circ\text{K}$, the value of τ_R was found to be temperature-independent for both samples and equal to 1.3×10^{-8} and 2.5×10^{-8} sec, respectively, the ratio of which equals the ratio of the residual resistivities. The results were obtained from measurements of the acoustomagnetoelectric effect (AME) at frequencies ranging from 6 to 35 MHz, in which high-frequency ultrasound sent longitudinally along a sample in a transverse magnetic field generates a dc electric field normal to both the magnetic field and the sound-propagation direction. The dependence of the AME on frequency and on the magnitude and direction of the magnetic field was measured and compared with the theory of Yamada. The temperature dependence of the ultrasonic attenuation coefficient α was also obtained. For $T \leq 20^\circ\text{K}$, the attenuation is mainly due to the interaction of the sound wave with carriers via the deformation potential, which interaction also produces the AME. For large magnetic fields, quantum oscillations similar to the de Haas-van Alphen effect are observed in both α and the AME voltage. Electron periods in the trigonal plane are identified. Finally, a lower bound for the deformation potential that describes the change of overlap of the electron and hole bands due to a trigonal compression is obtained: $|E_n - E_p| \geq 1.5$ eV.

I. INTRODUCTION

THE crystal structure of bismuth, a group-V semimetal, is a slight distortion from a simple-cubic Bravais lattice, with two atoms per unit cell.¹ The 10 electrons per unit cell would fill the fifth Brillouin zone were it not for a 0.036-eV overlap² with the sixth zone produced by the distortion. The result is a material which, at low temperatures, has 3×10^{17} electrons/cc equally distributed among the geometric-

louis zone were it not for a 0.036-eV overlap² with the sixth zone produced by the distortion. The result is a material which, at low temperatures, has 3×10^{17} electrons/cc equally distributed among the geometric-

* Submitted in partial fulfillment of the requirements for a Ph.D. degree at the Swiss Federal Polytechnic Institute (ETH), Zurich.

¹ H. Jones, Proc. Roy. Soc. (London) A147, 396 (1934).

² D. Weiner, Phys. Rev. 125, 1226 (1962); N. B. Brandt, T. F. Dolgolenko, and N. N. Stupochenko, Zh. Eksperim. i Teor. Fiz. 45, 1319 (1963) [English transl.: Soviet Phys.—JETP 18, 908 (1964)]; G. E. Smith, G. A. Baraff, and I. M. Rowell, Phys. Rev. 135, A1118 (1964); L. Esaki and P. J. Stiles, Phys. Rev. Letters 14, 902 (1965); G. A. Williams, Phys. Rev. 139, A771 (1965); R. N. Bhargava, *ibid.* 156, 785 (1967). See also Ref. 3.

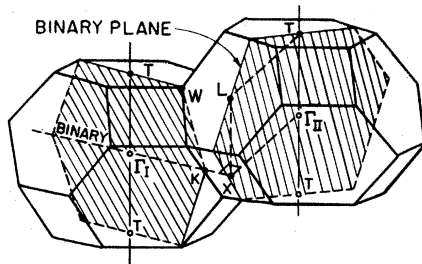


FIG. 1. Two adjacent Bi Brillouin zones showing planes, points, and directions of interest to the present experiments. Γ_I and Γ_{II} are equivalent points and are referred to generally as Γ .

ally equivalent conduction band minima located³⁻⁵ at L (shown in the reduced zone in Fig. 1), and an equal number of holes in the fifth zone located at the equivalent valence band maxima at T .³⁻⁵ (Recent band calculations including spin-orbit interactions by Golin⁶ indicate that Γ , the center of the reduced zone, is a possible alternative choice for the location of the hole band.)

It is of interest to ask what characteristic time determines the redistribution of electrons and holes between the two bands, and what microscopic mechanisms are involved. The transfer of an electron from the conduction band to the valence band (interband scattering), equivalent to the destruction of an electron-hole pair, involves a large crystal-momentum change, corresponding to the distance $TL = \Gamma X$ in Fig. 1 (or ΓL if the holes are located at Γ). It is not clear what supplies this momentum at temperatures well below the Fermi degeneracy temperature of the electrons and holes ($\sim 200^\circ\text{K}$).² Were it phonons, they would be either those phonons at X allowed by selection rules to couple T and L , or those at L which couple Γ and L ; the statistics together with the requirements of energy conservation would make a phonon process become progressively more improbable as the temperature is decreased. If this were the mechanism for recombination, we should be able to establish unequivocally the location of the hole band by comparing the experimentally derived phonon energies with the phonon dispersion data of Yarnell *et al.*⁷ and of Smith.⁸ Another

possibility is recombination in the presence of impurity centers. However, the reduction in Coulomb interactions due to the extremely large dielectric constant (~ 100), together with the available high purity of bismuth, should minimize the contributions of impurity centers, restricting their importance to very low temperatures.

The earliest attempts to measure τ_R were by Tosima *et al.*⁹ and by Schillinger.¹⁰ They tried to set up a spatially nonuniform distribution of electron-hole density by applying a fast rise time, high current pulse to a wire sample of bismuth, hoping to pinch the electron-hole plasma. The dynamics of the pinch would then be influenced by the generation of pairs at the outer edge of the pinch and by recombination at the center. From an analysis of the current-voltage characteristics, they estimated $\tau_R \gtrsim 10^{-8}$ sec at 80°K . Toxen *et al.*¹¹ estimated $\tau_R \sim 10^{-8}$ sec for one of their samples, from measurements on ultrasonic amplification in bismuth at 4°K .

Somewhat later, Zitter¹² obtained a value for τ_R of 1×10^{-8} sec at 4.2°K in a sample with $\rho_{300^\circ\text{K}}/\rho_{4.2^\circ\text{K}} = 360$ by a measurement of the photomagnetolectric effect (PME). In this experiment, excess electron-hole pairs are generated at the sample surface photoelectrically and allowed to diffuse inwards in the presence of a magnetic field. The Lorentz force on the diffusing electron and hole flux creates a transverse voltage, the PME voltage, which depends on τ_R .

The acoustoelectric effect (AE) has been shown by Weinreich *et al.*¹³ to be a powerful tool for obtaining information on intervalley scattering in germanium. In the AE effect, charged carriers are dragged along the propagation direction of externally imposed high frequency sound by the carrier-phonon interaction. The resultant charge build up at one end of the sample produces a longitudinal dc field, known as the acoustoelectric field (E_{AE}), if the densities of electrons and holes are unequal.¹⁴⁻¹⁸ It is quite clear that the relaxation time τ characteristic of the process that competes against the sound wave to restore the equilibrium carrier distribution will determine the magnitude of E_{AE} . For sound frequencies $\nu = \omega/2\pi$ such that $\omega\tau \ll 1$, the equilibrium distribution will be restored essentially instantaneously, while for frequencies such that $\omega\tau \gg 1$ the carrier distribution will be unaffected. Information on τ can therefore be obtained only for $\omega\tau \sim 1$, which requires that the sound frequency be in the megacycle

³ See, e.g., A. L. Jain and S. H. Koenig, *Phys. Rev.* **127**, 442 (1962); E. I. Blount and M. H. Cohen (unpublished), discussed by A. L. Jain, *Phys. Rev.* **114**, 1518 (1959).

⁴ S. Mase, *J. Phys. Soc. Japan* **13**, 434 (1958); **14**, 584 (1959); W. Harrison, *J. Phys. Chem. Solids* **17**, 171 (1960).

⁵ M. H. Cohen, L. M. Falicov, and S. Golin, *IBM J. Res. Develop.* **8**, 215 (1964); J. L. Hall and S. H. Koenig, *ibid.* **8**, 241 (1964).

⁶ S. Golin, *Phys. Rev.* **166**, 643 (1968); L. G. Ferreira, *J. Phys. Chem. Solids* **28**, 1891 (1967), has recently completed an augmented-plane-wave band calculation. His results on the character of the wave functions at L and T agree with Mase's results. Ferreira does not consider Γ as a possible alternative hole-band location, although his calculated energies and estimate of their relative error would allow it.

⁷ J. L. Yarnell, J. W. Warren, R. G. Wenzel, and S. H. Koenig, *IBM J. Res. Develop.* **8**, 234 (1964).

⁸ D. Smith (private communication); also D. Smith, Los Alamos Scientific Laboratory Report No. LA-3773, 1967 (unpublished).

⁹ S. Tosima and R. Hirota, *IBM J. Res. Develop.* **8**, 291 (1964).

¹⁰ W. Schillinger, *IBM J. Res. Develop.* **8**, 295 (1964).

¹¹ A. M. Toxen and S. Tansal (private communication).

¹² R. N. Zitter, *Phys. Rev. Letters* **14**, 14 (1965); **14**, 89 (E) (1965).

¹³ G. Weinreich, T. M. Sanders, and H. G. White, *Phys. Rev.* **114**, 33 (1959).

¹⁴ G. Weinreich, *Phys. Rev.* **104**, 321 (1956).

¹⁵ R. H. Parameter, *Phys. Rev.* **89**, 990 (1953).

¹⁶ E. I. Blount, *Phys. Rev.* **114**, 418 (1950).

¹⁷ N. Mikoshiba, *J. Phys. Soc. Japan* **15**, 1189 (1960); **16**, 895 (1961); *J. Appl. Phys.* **34**, 510 (1963).

¹⁸ S. G. Eckstein, *J. Appl. Phys.* **35**, 2702 (1964).

range for bismuth. For the case of equal numbers of electrons and holes, though their respective interactions with the phonons may be different, any charge separation (on the scale of the sonic wavelength) is opposed by the Coulomb fields which are set up; the result is an ambipolar drag and equal fluxes of negative and positive carriers, with essentially no AE effect.¹⁷ If a magnetic field is applied perpendicular to the direction of sound propagation, the electrons and holes will be deflected in opposite directions, producing an electric current in the third perpendicular direction. The dc field necessary to cancel this current is known as the acoustomagneto-electric field, E_{AME} . The possibility of observing this effect in bismuth was suggested to us by R. D. Brown of this laboratory. Independently, Yamada¹⁹ later reported the first experimental observation of the AME effect.

It is quite clear that the AME and AE effects give similar information about interband scattering. Under the appropriate circumstances, a measurement of either effect yields a value for the scattering time between separate band extrema in the Brillouin zone. In particular, for the case of bismuth, the AME will yield information exclusively on the electron-hole recombination only when a longitudinal sound wave is propagated along the trigonal direction (TTT in Fig. 1), since, by symmetry, the three electron bands are perturbed identically with respect to the hole band, and only transitions between any of these bands and the hole band will contribute to the AME effect. This was not the case for Yamada's geometry, used because of sample limitations, in which the mean time was measured for an electron to scatter out of one conduction minima simultaneously to other L points and to T (or Γ), with an uncertain weighting for each scattering; the time was estimated to be 3×10^{-8} sec at 4.2°K in a sample with $\rho_{300^\circ\text{K}}/\rho_{4.2^\circ\text{K}} \approx 200$.

Measurements on the AME effect as a function of frequency, temperature, and sample purity are reported here which yield much information on:

(1) The nature of the processes responsible for the recombination, and in particular, whether a single phonon process describes the recombination. A comparison of the activation energy derived from the AME effect with existing data on the phonon-dispersion curves in bismuth^{7,8} will be made in an effort to establish the exact location of the hole band. Furthermore, the phonon selection rules should yield a check on the symmetry labelling of the conduction band given by Mase.⁴

(2) The relative importance of impurity effects, not anticipated to be significant above $\sim 5^\circ\text{K}$ judging from measurements on the temperature dependence of the mobility.^{20,21}

(3) The contribution of electron-hole recombination

to the total scattering rate that determines electrical transport.

(4) The dominant mechanism of ultrasonic attenuation at low temperatures as determined by a comparison of the total attenuation α_{tot} and the magnitude of the AME effect. The origin of the oscillatory dependence of α_{tot} on magnetic field for high fields will be related to earlier conjectures.²²

(5) The effective deformation potential, compared with the results of Jain and Jaggi.²³

II. THEORETICAL CONSIDERATIONS

A sound wave of angular frequency ω and wave number \mathbf{k} produces a tensor strain in the crystal,

$$\epsilon = \epsilon_0 e^{i(\omega t - \mathbf{k} \cdot \mathbf{r})}, \quad (1)$$

which, for the geometry of the experiment reported here, will shift the relative positions of the conduction and valence band edges by an amount^{24,25} $(E_1 - E_2)\epsilon$, where E_1, E_2 are two elements of the general deformation potential tensor, and ϵ is the appropriate strain component.

If the symmetry of the strain allows for relative motion of degenerate or overlapping bands, the equilibrium carrier concentration in each band becomes a function of the local strain. As has been discussed in detail by Keyes²⁵ and by Adler,²⁶ and demonstrated experimentally by Bruner and Keyes,²⁷ the free energy of the carriers is altered by an amount which depends on the band parameters and is quadratic in the strain amplitude. This quadratic variation of the free energy represents an electronic contribution ΔC to the elastic constant and therefore to the sound velocity in the material.

If τ is a time that characterizes the local carrier concentration approach to equilibrium, then for $\omega\tau \sim 1$, the electronic contribution to the elastic constant C_0 becomes complex, the response becomes out of phase with the driving force, resulting in a contribution to the ultrasonic attenuation or dissipation.

It is straightforward to show that the additional attenuation α_e is given by^{26,28}

$$\alpha_e \approx \frac{\Delta C}{2C_0} \frac{\omega\tau}{1 + \omega^2\tau^2} \frac{\omega}{v_0}, \quad (2)$$

where τ is the characteristic time for restoration of the equilibrium carrier concentration n_0 , $v_0 = (C_0/\rho)^{1/2}$, and ρ is the density of the material. α_e will have a maximum when $\omega\tau = 1$ which will depend linearly on the frequency of the sound wave; α_e will be frequency-independent for $\omega\tau \gg 1$.

²² A. M. Toxen and S. Tansal, Phys. Rev. **137**, A211 (1965).

²³ A. L. Jain and R. Jaggi, Phys. Rev. **135**, A708 (1964).

²⁴ J. Bardeen and W. Shockley, Phys. Rev. **80**, 72 (1950).

²⁵ R. W. Keyes, IBM J. Res. Develop. **5**, 266 (1961).

²⁶ E. Adler, IBM J. Res. Develop. **8**, 430 (1964).

²⁷ L. Bruner and R. W. Keyes, Phys. Rev. Letters **7**, 55 (1961).

²⁸ M. Pomerantz, Proc. IEEE **53**, 1438 (1965).

¹⁹ T. Yamada, J. Phys. Soc. Japan **20**, 1424 (1965).

²⁰ Allen N. Friedman, Phys. Rev. **159**, 553 (1967).

²¹ R. L. Hartman (private communication).

In the steady state, the absorption of power from the sound field by the carriers, $S\alpha_e$ (W/cm³), where S is the sound energy flux, is balanced by a reaction of the carrier distribution. For carriers of one sign, the result is an effective electric field acting on the carriers E_{AE} , given by

$$v_0 e E_{AE} = S\alpha_e / N. \quad (3)$$

This expression, in which N is the carrier density, is often referred to as the Weinreich relation.²⁹ [See also Eq. (6b) of Ref. 16.] For the case of semimetals and the AME, Eq. (3) is readily modified to give¹⁹

$$E_{AME} = -(\mu H) E_{AE}, \quad (4)$$

where μ is an ambipolar mobility, and E_{AE} is the acoustoelectric field that would be produced if both carriers had the same sign of charge.

When the sound wavelength $2\pi/k$ is much greater than the carrier mean free path there are two important contributions to τ : (a) scattering between bands at a fixed point in space, characterized by the recombination time or interband scattering time τ_R , and (b) diffusion in space of carriers within one band along the density gradient produced by the sound wave, characterized by the time $(k^2 D_H)^{-1}$. Here D_H is the magnetic-field-dependent ambipolar carrier diffusion constant. From Yamada's¹⁹ Eq. (8) extended to low H , $\tau^{-1} = (\tau_R^{-1} + k^2 D_H)^{-1}$, where D_H is given by

$$D_H = (\sigma_n D_p + \sigma_p D_n) [\sigma_n (1 + (\mu_p H)^2) + \sigma_p (1 + (\mu_n H)^2)]^{-1}. \quad (5)$$

Yamada's Eq. (8) only holds for $k^2 D_H \ll \tau_R^{-1}$; it must otherwise be multiplied by $1 - 2k^2 D_H \tau_R$. (We have interchanged the notation τ and τ_R from Yamada's paper.) A measurement of the AME effect will yield information exclusively on the recombination time τ_R under experimental conditions such that $\tau_R^{-1} \gg k^2 D_H$. Since the primary purpose of the present experiment in bismuth is the determination of τ_R , one must establish experimental conditions such that

$$\tau_R^{-1} \gg k^2 D_H, \quad \omega \tau_R \sim 1 \quad (6)$$

are simultaneously satisfied. (The second condition was discussed in Sec. I.)

Blount¹⁶ has extensively studied the carrier-sound interaction in metals. For the case of two bands, as in bismuth, and $v_0/v_F \ll 1$ he obtains the following expression for α_e :

$$\alpha_e = \frac{|E_1 - E_2|^2 \omega^2 N_1 N_2}{2K v_0 (N_1 + N_2)^2} \times \frac{N_1 a_2 \tau_2 / (1 - a_2) + N_2 a_1 \tau_1 / (1 - a_1)}{1 + C_{12} [N_1 a_2 \tau_2 / (1 - a_2) + N_2 a_1 \tau_1 / (1 - a_1)]}, \quad (7)$$

where v_F is the Fermi velocity, K is an elastic constant,

²⁹ G. Weinreich, Phys. Rev. **107**, 317 (1957).

$C_{12}^{-1} = \tau_R (N_1 + N_2)$, N_i is the density of states at the Fermi level, and $a_i = (\tan^{-1} k l_i) / k l_i$, with l_i the carrier mean free path. The subscript $i=1, 2$ distinguishes the two bands. For the purpose of estimation, we assume $a_1 = a_2 = a$, $l_1 = l_2 = \tau / v_F$ with $\tau \approx 3 \times 10^{-10}$ sec³⁰, and $N_1 = N_2 = N$. Then

$$1/\alpha_e = C' (1/B\tau + 1/\tau_R), \quad (8)$$

where

$$C' = \frac{4K v_0}{|E|^2 \omega^2 N}, \quad B = \frac{a}{1-a}. \quad (9)$$

From Ref. 16,

$$\frac{a}{1-a} \approx \frac{\pi}{2kl} + \frac{b(kl)}{(kl)^2} + \dots \quad (10)$$

Here $b(kl)$ is a slowly varying function of kl that spans the interval $3 > b(kl) > 1.25$, for $0 \leq kl \leq \infty$. For the recombination to play a dominant role in α_e requires that

$$1/B\tau \ll 1/\tau_R, \quad (11)$$

from which it follows that

$$a/(1-a) \gg \tau_R/\tau \approx 30. \quad (12)$$

From Eqs. (9) and (1), we get $kl \ll 0.2$ or

$$\lambda \gg 30l. \quad (13)$$

We have to look for experimental conditions such that Eqs. (13) and (6) are satisfied. We consider the situation at 4°K.

Since $\tau_R \sim 10^{-8}$ sec, we have $\omega \tau_R \sim 1$ at ~ 12 MHz. The condition (6), $k^2 D \ll \tau_R^{-1}$, is readily satisfied for $H > 200$ Oe. To satisfy Eq. (13) is a bit more subtle. At 4°K and 12 MHz, $l \approx 6 \times 10^{-2}$ cm,³¹ $\lambda \approx 2 \times 10^{-2}$ cm, and $\lambda \approx \frac{1}{3} l$. One must reduce the effective carrier mean free path in the direction of the sound propagation so that it becomes much less than a wavelength. This can be accomplished by going to sufficiently high magnetic fields so that many cyclotron orbits are traced in a mean free path; i.e., to the limit of $(\mu_{\text{eff}} H)^2 \gg 1$. At $H = 5$ kOe, $(\mu_{\text{eff}} H)^2 \approx 3 \times 10^3$, and $\lambda \approx 10^3 l$ ($H = 5$ kOe), which readily satisfies Eq. (13).

A phenomenological theory for the AME effect developed by Yamada^{19,32} is applicable for $\mu H \gg 1$, but for H no so large that Landau quantization becomes important, and for sound waves of sufficiently low frequency such that $\omega \tau_e \ll 1$, where τ_e is the electron-phonon scattering time. Since $\tau_e \approx 3 \times 10^{-10}$ sec,³⁰ this condition is satisfied in bismuth for frequencies below 100 MHz for the whole temperature range reported here. The result is

$$E_{AME} = -\mu_{\text{eff}} H \frac{S}{\rho v_0^4 D} \left| \frac{E_1 - E_2}{e} \right|^2 \frac{\omega^2 \tau_R}{1 + \omega^2 \tau_R^2}. \quad (14)$$

³⁰ R. N. Zitter, Phys. Rev. **127**, 1471 (1962).

³¹ A. N. Friedman, J. J. Hall, and S. H. Koenig, Bull. Am. Phys. Soc. **4**, 169 (1959); D. H. Reneker, Phys. Rev. Letters **1**, 440 (1958); Phys. Rev. **115**, 303 (1959).

³² Cf. also A. A. Ginsberg, Fiz. Tverd. Tela **6**, 2010 (1964) [English transl.: Soviet Phys.—Solid State **6**, 1586 (1965)].

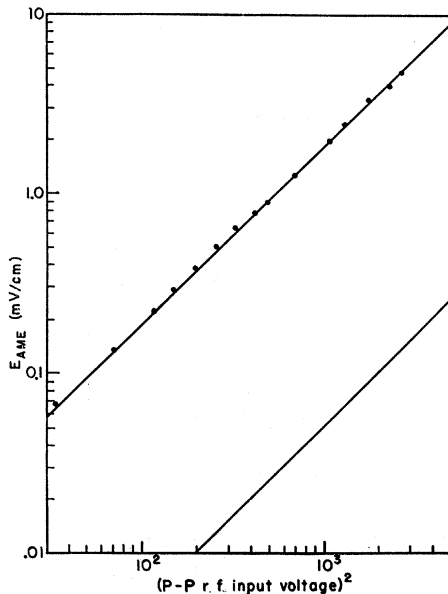


FIG. 4. Verification of the linear dependence of the E_{AME} on the sonic power flux predicted in Eq. (14). Lower curve shows results obtained in Ref. 19. The reasons for the difference in the two curves relates to the transducer efficiency and is discussed in the text.

powered by a regulated, slowly swept power supply. A model 120 Bell gaussmeter, calibrated against a NMR probe was used to determine the magnetic field strength to 1%.

A recording of the CRO traces (see Fig. 5), as well as peak values of $E_{AME}^{(+)}$ and $E_{AME}^{(-)}$ as a function of the magnetic field, for example, cf. Fig. 17) was obtained in the following way: By displaying the signal using the delaying sweep of the CRO, the main sweep can be used to sample parts of the total waveform displayed, and the “+ gate” output of the CRO can be used to generate a sampling pulse. A small modification, described by Mackey,³³ enables us to externally control the position of the + gate pulse with respect to the signal. The X axis of the X - Y recorder was fed either with a dc voltage proportional to the + gate position, or by the output of the gaussmeter. The “vertical output” of the CRO was fed into a gated integrator, a slight modification of the one described by Clark,³⁴ the gate of which was controlled by a Hewlett-Packard 212 pulser in turn triggered by the + gate. This procedure added flexibility in amplitude and length of the gating pulses. The output of the integrator was used to drive the Y axis of the recorder. With this arrangement, signals of the order of 1/20 the noise could easily be recovered and recorded as a function of either magnetic field or time.

The sample holder, see Fig. 6, inside a double-walled jacket (a single walled glass jacket was also used with similar results) was placed in a conventional system of

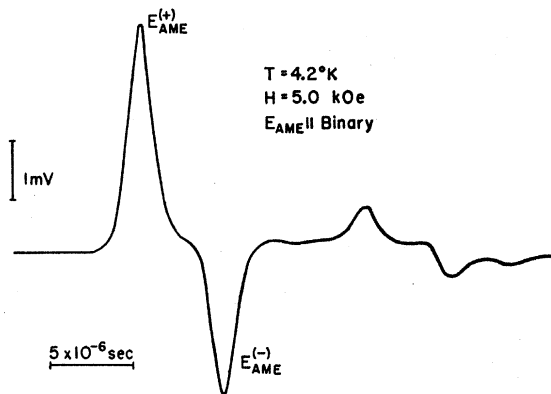


FIG. 5. Actual X - Y recorder trace of the E_{AME} in sample 1. Two double passages of the sonic pulse past the electrodes are easily recognizable ($\nu \approx 11$ MHz).

glass Dewars. Two Allen-Bradley 1/10-W resistors, with resistances $R_1(300^\circ\text{K}) \approx 1k\Omega$ and $R_2(300^\circ\text{K}) \approx 100\Omega$, were placed as close as possible to the sample (Fig. 6), and were used to measure temperatures above and below 4.2°K , respectively, using a 30-Hz Wheatstone bridge. Resistor R_1 , previously calibrated by J. J. Hall,³⁵ was checked at three temperatures: 4.2, 77, and 300°K . Resistor R_2 was calibrated against the He vapor pressure scale with standard Hg and oil manometers. By controlling the pressure of the He exchange gas in the jacket as well as the power input to a heater, any temperature above 4°K could be maintained constant during the few minutes necessary for a set of measurements. By pumping on the liquid-helium bath for approximately 20 min, temperatures down to 1.8°K could be attained. The maximum temperature uncertainty over the entire range was well below 1%.

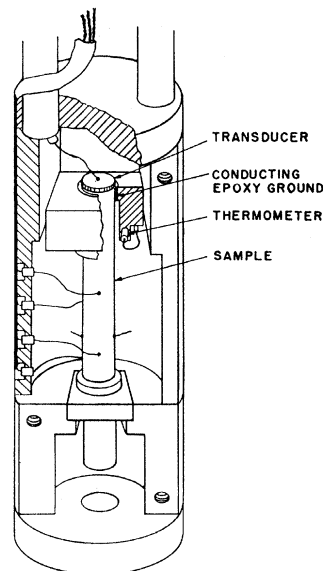


FIG. 6. Sample holder with sample 2 mounted. The heater and one of the thermometers are not shown.

³³ R. C. Mackey, Rev. Sci. Instr. **35**, 859 (1964).

³⁴ W. G. Clark, Rev. Sci. Instr. **35**, 316 (1964).

³⁵ J. J. Hall, Phys. Rev. **128**, 68 (1962).

TABLE I. Information about the two samples used.

Sample	$\rho_{300}^{\circ}\text{K}$	Dimensions	Sound propagation	E_{AME}
	$\rho_{4.2}^{\circ}\text{K}$			
1	260	2.1-cm length 0.635-cm diam	trigonal	binary
2	560	5.3-cm length 0.635-cm diam	trigonal	binary bisectrix

B. Samples

All measurements were performed on either of two samples cut from two large bismuth single crystals grown by a modified Bridgman technique³⁶ and made available by R. L. Hartman of this laboratory. Cylindrical samples, oriented lengthwise along the trigonal direction as determined by cleaving, were cut with a Servomet spark cutter. A special jig³⁷ allowed a sample to be cut well within 1° of the desired orientation with diameter uniform to 1 part in 10³ over the entire length. Some information on the samples is given in Table I. The samples were etched approximately 2 min in 35% nitric acid before cleaving both ends under liquid nitrogen. Cleaving proved to be the best way to obtain perfectly parallel and flat ends (flat compared to the sound wavelength $\lambda \geq 5 \times 10^{-3}$ cm) although one has to contend with the binary lines present on cleavage. Chemical polishing with a solution³⁸ containing six parts concentrated nitric acid, six parts glacial acetic acid and one part distilled water tended to introduce a slight curvature on a flat surface and was therefore discarded. By mechanically lapping the ends, polycrystalline layers of bismuth of considerable thickness (~ 0.1 mm) were formed. These layers introduced an additional source of acoustic attenuation and reduced the amount of sonic energy flux reaching the electrodes. The transducer end of sample 1 was mechanically lapped, which accounts, in part, for the difference in temperature range of the measurements reported on the two samples.

Since the distance from the near end to the electrodes in sample 1 was ~ 1.5 cm, which required rf pulses < 5 μsec , measurements of E_{AME} with the model 103 Keithley preamp were not possible because of its limited high-frequency response. Its low noise characteristics thus could not be utilized, in contrast to the case for sample 2, where the pulses were ~ 15 μsec . The other two detecting systems had about five times the input noise level of the 103 Keithley preamp, which further reduced the temperature range over which the AME effect could be observed in sample 1.

A PZT-4 transducer of ~ 10 MHz mean frequency (0.635 cm diam) was cemented to the near end of the samples with Dow-Corning Silicone fluid of viscosity 2.5×10^5 centistokes (Dow-Corning Corporation, Mid-

³⁶ R. D. Brown III, IBM J. Res. Develop. **10**, 462 (1966).

³⁷ Kindly made available to us by R. L. Hartman of this laboratory.

³⁸ L. C. Lovell and J. H. Wernick, J. Appl. Phys. **30**, 234 (1959).

TABLE II. Sound velocities in 10⁵ cm/sec, at Γ , for various directions of propagation.

Direction of propagation	v_{LA}	v_{TA}	v_{TA}
ΓL	2.40	1.51	1.15
ΓX	2.56	1.02 ^b	0.972
ΓT^a	1.972 ^c	1.074 ^b	1.074 ^b
ΓKX	2.55	1.55	0.848

^a Reference 39.

^b Pure transverse.

^c Pure longitudinal.

land, Michigan). This type of transducer was used in preference to quartz because of its high electromechanical coupling constant (about four times that of quartz); its conversion efficiency is as high as 30% over a fairly broad frequency interval centered about its resonant frequencies. The advantage gained is shown in Fig. 4. The transducer was driven at the fundamental frequency ν_0 , at some frequencies well above and below ν_0 , and at the third harmonic (~ 35 MHz).

Electrical contacts were made by soldering #36 bare copper wire to the sample with Bi-Cd solder and #272 Divco flux. Twisted pairs of #32 Formvar insulated copper wires provided electrical connection to the detecting systems. The binary lines on the cleavage plane were used to align the contacts with the binary and bisectrix directions.

The samples were mounted in a manner similar to the description in Ref. 13 with two differences (see Fig. 6): (a) Eccobond 57C (Emerson and Cumming, Inc.), an electrically conducting epoxy with volume resistivity $< 6 \times 10^{-4}$ Ω cm provided both a ground path for the rf and a mechanical support for the sample. By diluting Eccobond 57C in toluene and extremely thin uniform epoxy coating of the sample grounding area was obtained with $\sim 5 \times 10^{-3}$ cm clearance between the copper collar and the sample. The samples were never removed from their collars for the duration of the experiments. The epoxy was allowed to cure for more than 12 h at room temperature. No evidence of sample damage due to differential thermal expansion could be detected even after repeated temperature cyclings. Some shear-mode conversion due to clamping by the epoxy apparently occurs, judging from the "bump" immediately before $E_{\text{AME}}^{(-)}$ for sample 2 and immediately after $E_{\text{AME}}^{(-)}$ for sample 1 in Fig. 3, since the transverse sound velocity is about half the longitudinal velocity (cf. Table II).³⁹ (b) No absorber was soldered to the far end of the sample, which would prevent the sonic pulses from being reflected.

IV. EXPERIMENTAL RESULTS

A. Temperature Dependence of Electron-Hole Recombination Time

The temperature dependence of E_{AME} normalized and corrected for attenuation (see below) at various

³⁹ Y. Eckstein, A. W. Lawson, and D. H. Reneker, J. Appl. Phys. **31**, 1534 (1960).

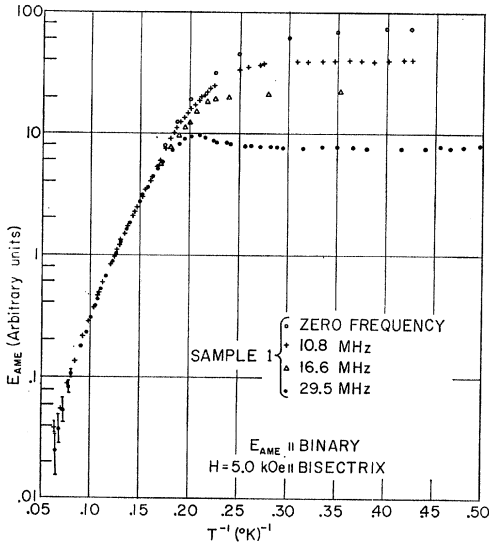


FIG. 7. Raw E_{AME} corrected for acoustic attenuation and normalized in the temperature range where $\omega\tau < 1$. The zero-frequency curve refers to Eq. (14).

frequencies for both samples, is shown in Figs. 7 and 8. We have chosen to normalize the data for the various frequencies by shifting the vertical scale to make the data overlap over the widest temperature range. It is clear from Eq. (14) that such an overlap is only possible in the temperature range where $\omega\tau_R \ll 1$ or $\omega\tau_R \gg 1$; we have chosen the former range. The data show that E_{AME} decreases rapidly with increasing temperature and is independent of sample purity for $T \geq 8^\circ\text{K}$. This is not true for $T < 8^\circ\text{K}$, indicating that some mechanism which can probably be associated with the sample purity plays a role at these temperatures; its relative importance with respect to what could be called the main process for recombination will vary from sample to sample as it does indeed for our two samples. The main feature of this process is to make E_{AME} temperature-independent, so that τ_R will reach a saturation value τ_R^{sat} below $\sim 3^\circ\text{K}$, which will depend primarily on the sample purity.

In Fig. 8, E_{AME} measured on sample 2 for two sets of contacts along directions parallel to the binary and bisectrix axes is shown. The data have been displaced for clarity. The temperature dependence of the AME is the same for both orientations, though there is a small anisotropy in the absolute magnitude of E_{AME} , as shown in Fig. 9. The explanation for this fact involves the anisotropy of the ambipolar effective mobility μ_{eff} , and will be discussed subsequently.

Any frequency dependence of E_{AME} , as shown in Figs. 7 and 8, has to come from the factor $(1 + \omega^2\tau_R^2)^{-1}$ in Eq. (14). The functional form of the predicted frequency dependence has been verified by taking measurements at three frequencies, and therefore the data for two frequencies at a fixed temperature below $\sim 8^\circ\text{K}$ can be used to compute $\tau_R(T)$. The results are

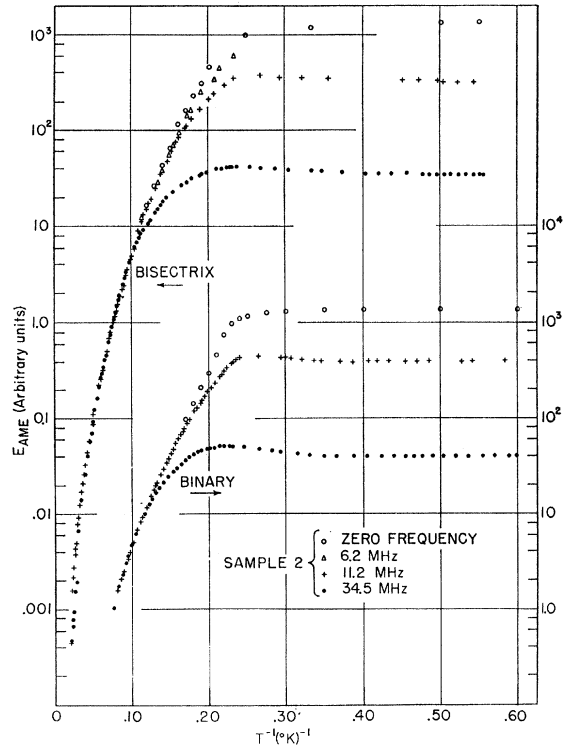


FIG. 8. Raw E_{AME} corrected for acoustic attenuation and normalized in the temperature range where $\omega\tau < 1$. Shown are results obtained for contacts along a bisectrix direction (read left scale) and binary direction (read right scale) in sample 2. Data have been displaced vertically for clarity. $H = 5.0$ kOe.

presented in Fig. 10 and confirm, within the experimental error, what has been said above with regard to the low-temperature saturation of τ_R :

$$\begin{aligned} \text{sample 1, } \tau_R^{sat} &= (1.30 \pm 0.13) \times 10^{-8} \text{ sec,} \\ \text{sample 2, } \tau_R^{sat} &= (2.50 \pm 0.25) \times 10^{-8} \text{ sec.} \end{aligned}$$

In order to obtain $\tau_R(T)$ for the full temperature range of the present experiments, a knowledge of the

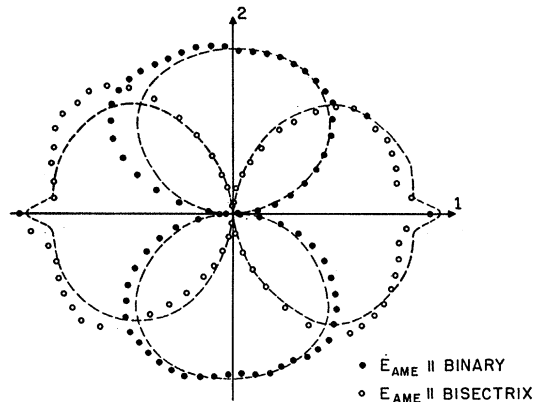


FIG. 9. Angular dependence of E_{AME} for contacts along the binary and bisectrix directions in sample 2 obtained by rotating the magnetic field in the trigonal plane. $H = 540$ Oe, $T = 4.2^\circ\text{K}$.

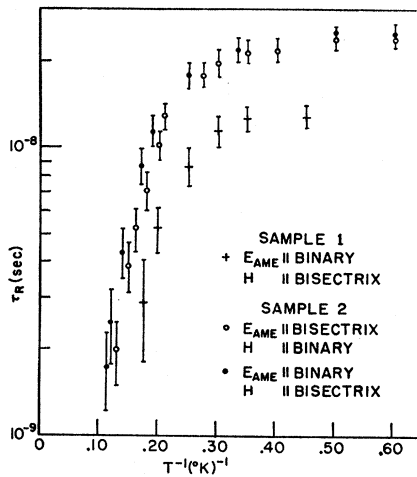


FIG. 10. Electron-hole recombination time for samples 1 and 2 versus T^{-1} , obtained from the frequency-dependent part of $E_{AME}(T)$ shown in Figs. 7 and 8.

temperature dependence of μ_{eff} is required. $\tau_R(T)$ can be determined independently of μ_{eff} as long as there is a frequency dependent E_{AME} of the kind shown in Figs. 7 and 8. By multiplying any $E_{AME}(\omega)$ by $1 + \omega^2 \tau_R^2$, a quantity proportional to $\mu_{\text{eff}}(T)$, the zero frequency E_{AME}^0 curve is obtained,

$$E_{AME}^0(T) \propto \mu_{\text{eff}}(T) \tau_R(T), \quad (15)$$

which yields the T variation of $\mu_{\text{eff}}(T)$ for $T \leq 8^\circ\text{K}$. The results for samples 1 and 2 are shown in Fig. 11, together with the results on the temperature dependence of some components of the resistivity tensor obtained by Friedman²⁰ and by Hartman.²¹ Friedman's data were interpolated to our resistivity ratios of 260 (curve A),

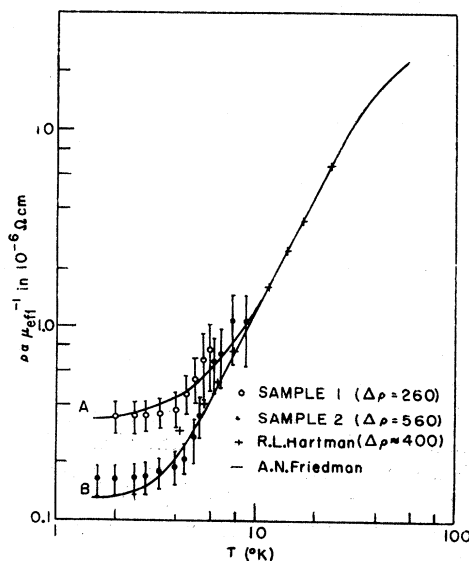


FIG. 11. Temperature dependence of $\mu_{\text{eff}} \approx \nu_3$ as obtained from Fig. 10 and Eq. (15). Also shown are experimental results reported in Refs. 20 and 21 for two components of the resistivity tensor, ρ_{11}^0 and ρ_{33}^0 .

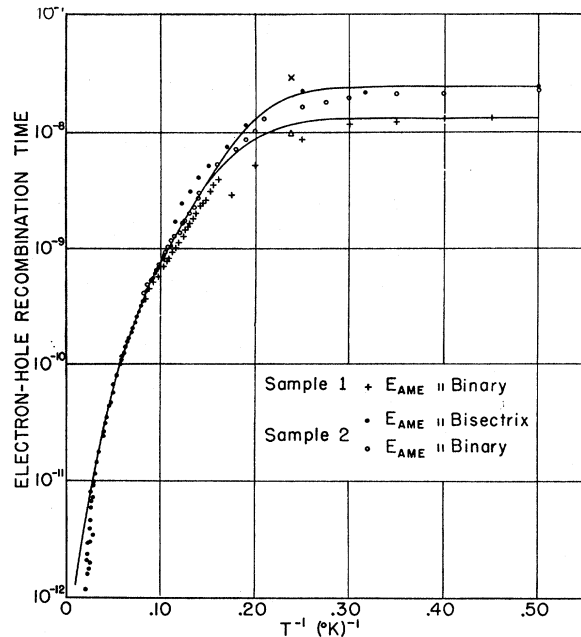


FIG. 12. Temperature dependence of the electron-hole recombination in samples 1 and 2 obtained as described in the text. The solid curves refer to Eqs. (25)–(27). Δ , Ref. 12; X , Ref. 19.

and 560 (curve B). Hartman's sample is thought to have a resistivity ratio of ≈ 400 . The agreement of the present data on $\mu_{\text{eff}}(T)$ with those of these two authors, we believe, justifies the extrapolation of $\mu_{\text{eff}}(T)$ to higher temperatures as given by the solid curve in Fig. 11. This shows that for most of our temperature range, $\mu_{\text{eff}}^{-1} \propto T^2$, which is characteristic of all measured components of the resistivity tensor, though as of now not fully understood.^{20,21}

From Eq. (15), curves A and B of Fig. 11 for samples 1 and 2, respectively, and the corresponding values for τ_R^{sat} , $\tau_R(T)$ at all temperatures can be obtained. The results, shown in Fig. 12, indicate a strong temperature dependence of τ_R , independent of sample purity above $\sim 8^\circ\text{K}$. (This is also the case for $\mu_{\text{eff}}(T)$; see Fig. 11.) The solid curve represents the theoretical model proposed and discussed in the next section.

B. Acoustic Attenuation

Figures 13 and 14 show the results of the temperature and frequency dependence, at various magnetic fields, of the attenuation coefficient α obtained in the manner described in Sec. III. Temperature-independent dispersion losses (due to beam divergence) were evaluated, assuming the transducer acts as a piston source and the sample as a waveguide,⁴⁰ and were subtracted from the measured losses. An estimated $\pm 20\%$ uncertainty is introduced when comparing the attenuation at various frequencies for a fixed temperature by this procedure, while the experimental error in $\alpha(T)$ at a fixed frequency is $< 5\%$. The following conclusions can be

⁴⁰ M. Redwood, Proc. Phys. Soc. (London) 70, 721 (1957).

drawn from the experimental results: (a) Electron-hole recombination is the major mechanism for acoustic attenuation in our very pure samples, in contrast with Yamada's observations¹⁹ on less pure material, as indicated most obviously by the maxima in the attenuation which occur at $\omega\tau_R=1$, within the experimental uncertainty. The prediction of Eq. (2) that the maximum attenuation is proportional to ω , is also (roughly) satisfied by the experimental results. (b) From Eq. (2), $\tau^{-1}=\tau_R^{-1}+k^2D_H$. At 4°K, for $\nu=6$ MHz and $H=5$ kOe, $\tau_R\approx 10^{-8}$ sec, $D_H\approx 1$ cm²/sec, and $k=200$ cm⁻¹. Therefore $k^2D_H\ll\tau_R^{-1}$, $\tau=\tau_R$, and one concludes that the diffusion term does not contribute to the attenuation at high magnetic fields. On the other hand, for $H=15$ Oe, $k^2D_H>\tau_R$ and $\tau\approx k^2D_H^{-1}$ and the diffusion term dominates the AME. From the experimental results for $\nu=6$ MHz, we have

$$\alpha_{\text{tot}}(5 \text{ kOe})/\alpha_{\text{tot}}(15 \text{ Oe})\approx 2,$$

although

$$\tau(5 \text{ kOe})/\tau(15 \text{ Oe})\geq 10.$$

Therefore the diffusion contribution, though it dominates the recombination contribution to α_e , only represents $\sim 20\%$ of the total attenuation at very low magnetic fields, with the remainder unassociated with α_e . This remainder is a temperature-independent contribution to the acoustic attenuation which appears to decrease with increasing sample purity and perfection. (c) Since α_e does dominate the total attenuation for $\mu_{\text{eff}}H\gg 1$, an experimental verification of Eq. (6), the "modified Weinreich relation" is in principle possible. With typical values of E_{AME} and S (there is approximately 50% uncertainty in S), Eq. (6) predicts $\alpha_e\approx 0.15$ cm⁻¹ at $H=5$ kOe, compared with $\alpha_{\text{tot}}\approx 0.25$ cm⁻¹ measured directly at 5 kOe and 11 MHz. This must be considered good agreement under the circumstances; in particular, the conclusion is that the experimental magnitude of α agrees with the magnitude anticipated

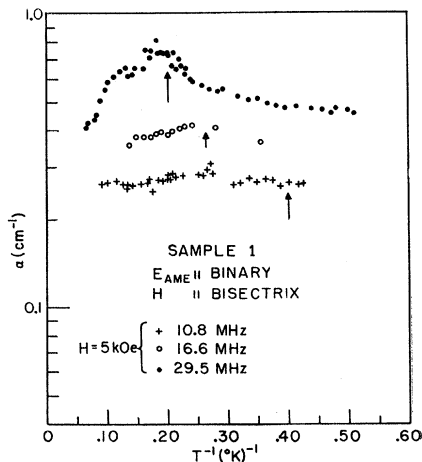


FIG. 13. Temperature and frequency dependence of the total attenuation coefficient α_{tot} in sample 1, corrected for dispersion losses. Arrows indicate temperature at which $\omega\tau_R=1$.

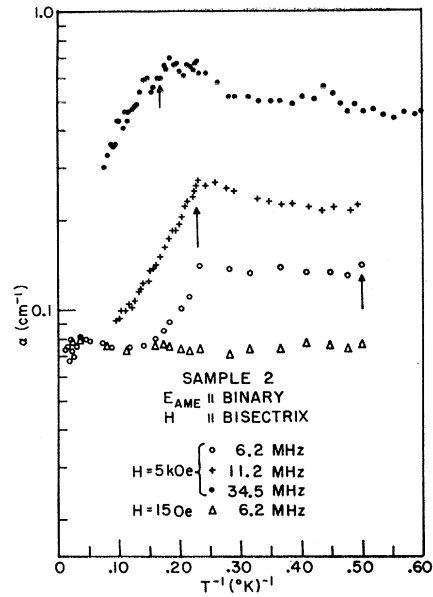


FIG. 14. Temperature and frequency dependence of the total attenuation coefficient α_{tot} in sample 2 corrected for dispersion losses. Data for $\nu=6.2$ MHz were obtained from the rf echo pattern. Arrows indicate temperature at which $\omega\tau_R=1$.

from the interband recombination mechanism, reinforcing conclusion (a) above.

C. Deformation Potential

An accurate measurement of the deformation potential is possible only if, as in the case of obtaining α_e , the difficulty of obtaining precise measurements of the sonic energy flux S sent along the crystal can be overcome. A lower limit for $|E_1-E_2|$ was obtained as follows: For a fixed energy flux $S>1$ W/cm², the sample chamber temperature was measured. With the rf power then turned off, the temperature rise due to S was reproduced using the heater. An upper limit for S was obtained in this manner since not all the heating due to the rf pulse results from the absorption of the ultrasound in the sample. From Eq. (14), we obtain

$$|E_1-E_2|\geq 1.5 \text{ eV},$$

in good agreement with the results of Jain and Jaggi,²³ who give $|E_1-E_2|=2.5$ eV.

D. Magnetic Field Dependence of AME

The preceding results were obtained for values of magnetic field sufficiently low so that quantum effects were small, though, in general, not negligible. The linear dependence of the AME on H predicted by Eq. (14) holds over a limited range of magnetic fields (see Figs. 17 and 20). Both quantum effects, which become more pronounced at lower temperatures (see Fig. 17), and deviations associated with the deviation from the ideal H^2 dependence of the magnetoresistance, are observed experimentally. The latter introduces a small systematic

error in the measurements of $E_{\text{AME}}(T)$ when measurements versus temperature are made at a fixed magnetic field, since $\mu_{\text{eff}}H$ is temperature-dependent. As the temperature is raised, the quantum oscillations disappear and one gets progressively closer to the strictly linear region. An estimate of this error can be made by measuring the AME effect at two fields as a function of temperature (for our case 5 and 2 kOe). It was found to be under 10% at the lowest temperatures, decreasing monotonically with increasing temperature. A correction is included in Figs. 7 and 8.

Oscillatory quantum effects are observed both in E_{AME} and in $\alpha_e \simeq \alpha_{\text{tot}}$. These results will be presented and discussed separately, in Sec. VI, since they do not bear directly on τ_R , the main subject of this investigation.

V. DISCUSSION

A. Phonon Interaction

The strong temperature dependence of τ_R (Fig. 12) above $\sim 8^\circ\text{K}$, the same for both samples, suggests that the mechanism of electron-hole recombination involves an interaction in which a single, energetic phonon with wave vector necessary to conserve crystal momentum, is either emitted or absorbed. Under the appropriate conditions, such a recombination process can be characterized by a relaxation time τ_R . Let overlapping electron and hole bands be displaced due to a perturbation which instantaneously shifts the bands relative to each other, so that the carrier density in each band differs from its equilibrium value n_0 by an amount $n_1' = -n_2'$, where the subscript 1 refers to the electron band, and 2 to the hole band. The time rate of change of the excess carrier density is then

$$dn_1'/dt = R_{12} - R_{21}, \quad (16)$$

where R_{12} is the total transition rate of electrons from the electron band to the hole band, and R_{21} is the reverse rate. We would like

$$R_{12} - R_{21} = -\frac{n_1'}{\tau_{12}} + \frac{n_2'}{\tau_{21}} = -n_1' \left(\frac{1}{\tau_{12}} + \frac{1}{\tau_{21}} \right) = -\frac{n_1'}{\tau_R} \quad (17)$$

to hold, with τ_R independent of n_1' . If M is the matrix element for the scattering of an electron to the hole band with either the emission or absorption of the phonon with the required momentum, and associated energy $\hbar\omega$, then the total rate R_{12} , from first-order perturbation theory, is

$$R_{12} = \frac{2\pi}{\hbar} \left(N \int_{-\infty}^{\infty} |M|^2 g_1(\epsilon) g_2(\epsilon + \hbar\omega) f_1(\epsilon) \times [1 - f_2(\epsilon + \hbar\omega)] d\epsilon + (N+1) \int_{-\infty}^{\infty} |M|^2 g_1(\epsilon) \times g_2(\epsilon - \hbar\omega) f_1(\epsilon) [1 - f_2(\epsilon - \hbar\omega)] d\epsilon \right), \quad (18)$$

where ϵ is the energy of the electrons and N is the Bose function for phonons of energy $\hbar\omega$. The two terms represent the contributions from phonon absorption and emission, respectively. The distribution functions f_i , $i=1, 2$, may be written as

$$f_i(\epsilon) = f_0(\epsilon) + f_i'(\epsilon) \simeq f_0 + \xi_i' (\partial f_0 / \partial \xi)_{\xi=\xi_0} \simeq f_0 - (\xi_i' / kT) f_0 (1 - f_0) \quad (19)$$

for f_i' and n_i' small, where $\xi_i' = n_i' / g_i(\xi_0)$ is the perturbation in Fermi energy of the i th band from its equilibrium value ξ_0 , and g_i is the density of states. Since for $f_i' = 0$, $R_{12} = R_{21} = 0$, one can readily derive the result for τ_R^{-1} ,

$$\frac{1}{\tau_R} = \frac{4\pi}{\hbar} \left(N \int |M|^2 g_1 g_2 [f_1'(\epsilon) - f_2'(\epsilon + \hbar\omega)] d\epsilon \times \int [g_1 f_1'(\epsilon) - g_2 f_2'(\epsilon + \hbar\omega)] d\epsilon + (N+1) \int |M|^2 g_1 g_2 [f_1'(\epsilon) - f_2'(\epsilon - \hbar\omega)] d\epsilon \times \int [g_1 f_1'(\epsilon) - g_2 f_2'(\epsilon - \hbar\omega)] d\epsilon \right). \quad (20)$$

If we assume $\xi_i' \ll \xi_0$, and write g_i^0 for $g_i(\xi_0)$, then

$$\frac{1}{\tau_R} = \frac{2\pi}{\hbar} |M|^2 \left(\frac{g_1^0 + g_2^0}{g_1^0 g_2^0} \right) \left(N \int_{-\infty}^{\infty} g_1(\epsilon) g_2(\epsilon + \hbar\omega) f_1(\epsilon) \times [1 - f_2(\epsilon + \hbar\omega)] d\epsilon + (N+1) \int_{-\infty}^{\infty} g_1(\epsilon) \times g_2(\epsilon - \hbar\omega) f_1(\epsilon) [1 - f_2(\epsilon - \hbar\omega)] d\epsilon \right). \quad (21)$$

So long as the $g_i(\epsilon)$ do not vary appreciably over the energy range kT about the maximum of the function $f_0(\epsilon)[1 - f_0(\epsilon \pm \hbar\omega)]$, which in principle means so long as the Landau quantization of the levels is not too severe, they may be removed from under the integral to give the result

$$\frac{1}{\tau_R} = \frac{2\pi}{\hbar} (g_1^0 + g_2^0) |M|^2 \frac{x}{\sinh^2 x}. \quad (22)$$

Here $x = \hbar\omega / 2kT = T_p / 2T$, and T_p is the phonon energy in $^\circ\text{K}$. For $x \gg 1$, Eq. (22) can be approximated by

$$\tau_R^{-1} \propto 2xe^{-2x}; \quad (23)$$

the AME then has an activation energy given by kT_p . For $x \ll 1$,

$$\tau_R^{-1} \propto x^{-1} \propto T. \quad (24)$$

Over the range $6\text{--}20^\circ\text{K}$, it was found that a phonon energy of $\hbar\omega/k = 43^\circ\text{K}$ fits the data. Above 20°K ,

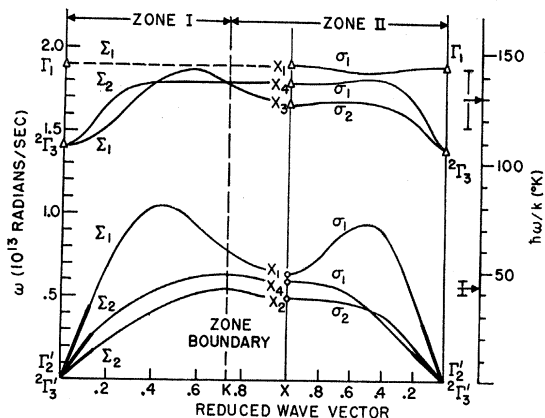


FIG. 15. Solid curves: phonon-dispersion curves for propagation along the binary direction (ΓKX) from Refs. 7 and 8, and along ΓX from Ref. 8. The slopes of the straight lines at the zone center were calculated from the sound velocities (see Table II). Dashed curve is conjectured. Only the two σ_2 branches are pure modes (transverse). Δ and \circ indicate optical phonons and acoustic phonons, respectively. The arrows at the right indicate our activation energies, Eq. (25).

another energy appears to be present; the experimental data above 6°K could be fit within the experimental error by the sum of two functions as in Eq. (22), with the following two phonon energies:

$$T_{p_1} = (43 \pm 4)^\circ\text{K}, \quad T_{p_2} = (130 \pm 15)^\circ\text{K}. \quad (25)$$

Below $\sim 8^\circ\text{K}$, the data depend on the sample purity; at the lowest temperatures, impurity scattering, characterized by a temperature-independent scattering time τ_I , is the dominant recombination process. Therefore, the recombination time is given by

$$\frac{1}{\tau_R} = A \frac{x_1}{\sinh^2 x_1} + B \frac{x_2}{\sinh^2 x_2} + \frac{1}{\tau_I}, \quad (26)$$

where A and B are constants that measure the strength of the interaction with the two different phonons. The final fit gives

$$\begin{aligned} A &= 1.09 \times 10^{10} \text{ sec}^{-1}, \\ B &= 5.35 \times 10^{11} \text{ sec}^{-1}, \\ \tau_I^{-1} &= 7.52 \times 10^7 \text{ sec}^{-1} \quad (\text{sample 1}), \\ \tau_I^{-1} &= 4.00 \times 10^7 \text{ sec}^{-1} \quad (\text{sample 2}), \\ x_1 &= 21.5/T, \\ x_2 &= 65/T. \end{aligned} \quad (27)$$

B. Phonon Spectra and Selection Rules

The activation energies, Eq. (25), must correspond to the energies of phonons with momenta equal to the separation in momentum space of the conduction and valence bands. In addition, the coupling of the two bands by the phonons must be allowed by symmetry. If one knew with more certainty the symmetry of the electronic levels, the present results, combined with the

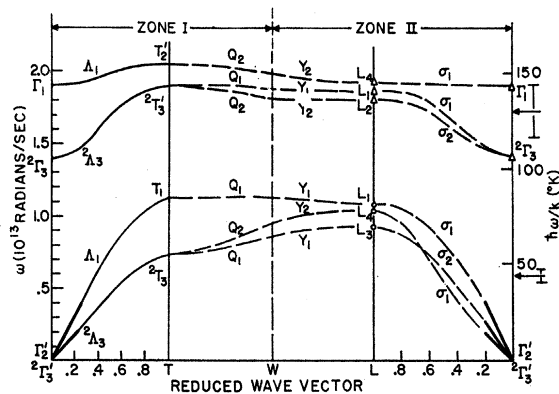


FIG. 16. Solid curves, phonon-dispersion curves for propagation along the trigonal direction (ΓT) (Ref. 7), along TWL and ΓL (Ref. 8). Again the slopes at Γ are obtained from the sound velocities (see Table II). The notation is as in Fig. 15. Along ΓL all modes are pure. Along ΓL only the two σ_2 are pure modes (transverse). The arrows indicate our activation energies, Eq. (25). Dashed curves are conjectured.

recently completed data on the phonon spectra in bismuth,⁸ would allow one to determine unequivocally whether the valence band is at Γ or T . As pointed out in Sec. I, no calculation or experiments to date have been able to settle this point. If the valence band is at T , both vectors ΓX and ΓKX couple the bands, and one is interested in phonons at X . If the valence band is at Γ , one is interested in phonons at L (cf. Fig. 1). Our data, in combination with phonon energies obtained by Smith⁸ at X and L (see Figs. 15 and 16), show that the valence band maximum is at T ; the value $T_p = 43^\circ\text{K}$ (also as reported earlier⁴¹), is in excellent agreement with an acoustic phonon^{7,8} at X , while the value $T_p \approx 130^\circ\text{K}$ would correspond to an optical phonon at X .⁸ It remains to be determined whether these phonons are allowed by symmetry to couple the conduction and valence bands.

There have been two calculations of the electronic structure of bismuth, one a tight-binding computation, by Mase,⁴ the other a pseudopotential band calculation by Golin.⁶ Both, though they include spin-orbit interaction (~ 1 eV for bismuth⁴²), suffer from the difficulty that the properties of bismuth are determined by the relative positions of bands within an energy range that is of the order of, or less than, the uncertainty in the calculations.

Mase gives the symmetry of the conduction band at L as $L_6 + L_6$ (even under inversion), and that of the valence band⁴³ at T as $T_4' + T_6'$ (odd under inversion)

⁴¹ A. A. Lopez and S. H. Koenig, Solid State Commun. 4, 513 (1966). Because of a slight oversight, the upper right-hand diagram in Fig. 1 is in error. The positive Y axis should point in the opposite direction. Furthermore, the angles should read $YL' = -25^\circ 48'$, $YT_1 = +59^\circ 30'$; with the corresponding orthogonal modes at 90° to these. ΓX remains unchanged.

⁴² E. U. Condon and G. H. Shortley, *The Theory of Atomic Spectra* (Cambridge University Press, Cambridge, England, 1951).

⁴³ See also G. E. Smith, G. A. Baraff, and J. M. Rowell, Phys. Rev. 135, A1118 (1964).

in terms of the representations of the double group.⁴⁴ Golin, by computing the g value of the various valence bands and comparing with the experimental data,⁴³ gives the symmetry $\Gamma_4 + \Gamma_5$ (even under inversion) if the maximum is at Γ , and is in agreement with Mase if the maximum is at T . He does not give the conduction band symmetry. In order to determine the selection rules, one must determine the irreducible representations contained in the direct product of the representation of the valence and conduction bands, and see if this reduction contains the appropriate phonon representation. We consider the two cases, corresponding to the valence band maxima at T and Γ , separately.

1. Valence Band Maxima at T

If the valence band maxima is at T , we are interested in the phonons at X . Since the symmetry group at X (and at L as well) is a four-element, Abelian group, the irreducible representations are one-dimensional and the reduction of the direct product is particularly simple. The four product wave functions of the form $(\psi_C^*)(\psi_V)$ that can be formed from functions with symmetry ψ_{C,L_5} , ψ_{C,L_6} , $\psi_{V,T_4'}$, and $\psi_{V,T_5'}$, where the subscripts C and V refer to conduction and valence bands, turn out to be basis functions for a four-dimensional representation of the group at X . From the table of characters in Mase, this representation is readily obtained and reduced to the result

$$(L_5 + L_6) * (\Gamma_4 + \Gamma_5) = 2(X_3 + X_4). \quad (28)$$

The phonons at X cannot be labeled unequivocally without regard either to a good force-constant model or experimental data which show how the different phonons connect at X . The labeling of the modes between Γ and X can be obtained by requiring that the symmetry of the motion near Γ look like long-wavelength acoustic or optic modes, in addition to satisfying the requirements of crystal symmetry. For propagation along $\Gamma K X$, a twofold axis, the phonons must be odd or even with respect to a rotation of 180° . For propagation along ΓX , the phonons must be odd or even with respect to reflection in the mirror plane. From these considerations, one obtains the labeling of these modes as shown in Fig. 15. The labeling agrees also with the computations of Smith.⁸ The phonon data and force-constant model in Ref. 8 require that the X_2 energy be less than the X_3 energy; from this and the compatibility relations given by both Mase and Golin, the labeling at X follows. There is still the possibility of X_1 and X_4 being interchanged if Σ_1 and Σ_2 cross along $\Gamma K X$. Thus from Eq. (28), assuming the labeling of the conduction band to be correct, phonon-aided recombina-

tion of electrons and holes is allowed in first order by interaction with one acoustic and two optical phonons at X .

2. Valence Band Maxima at Γ

The phonons that couple Γ and L are L phonons. However, the labeling of the phonons at L is not so straightforward as at X . In particular, the symmetry alone does not require that the T_1 LA phonon connect with the LA phonon at L (Fig. 16), though intuition suggests this. The T_1 , Q_1 , Y_1 branch can in principle connect to σ_2 at L , as can the branch 2T_3 , Q_1 , Y_1 . That is, either of the Q_1 , Y_1 branches can cross the Q_2 , Y_2 branch along TWL , but of course not each other. The force-constant model given in Ref. 8 requires that the L_2 energy be greater than the L_3 energy; the labeling at L is then unique except again for the order of L_1 and L_4 as was the case at X . Our labeling at T is also compatible with the force-constant model.

From the direct product of the band representations, we find the reduction to be

$$(L_5 + L_6) * (\Gamma_4 + \Gamma_5) = 2(L_1 + L_2), \quad (29)$$

again allowing one acoustic and two optical phonons to make a first-order contribution to the electron-hole recombination.

From our measured activation energies and the phonon data^{7,8} we can ascertain that the principal valence band is located at T ; there are no modes at L close to 43°K . In addition, the allowed mode at L is the highest energy acoustic mode. However, we cannot rule out the possibility of another hole band either at Γ or elsewhere in the zone (since optical phonon energies are similar throughout the Brillouin zone^{7,8}) with its maximum approximately 19 meV below the Fermi surface, the energy corresponding to 130°K . There is some circumstantial evidence for such a band.⁴⁵ Mase's conduction band labeling cannot be unequivocally verified, since if we were to choose $L_7 + L_8$ (odd under inversion) for the labeling of the conduction band, the phonon-selection rules at X would be $X_1 + X_2$, also compatible with our results. We favor Mase's labeling though, since from Eq. (27), $B \gg A$, indicating that at sufficiently high temperatures electron-hole recombination takes place preferably with emission or absorption of a 130°K phonon. This could indicate that a greater number of 130°K phonons is involved, compared with the number of 43°K phonons. Mase's conduction-band labeling allows four 130°K phonons (two at X and two at L) and one 43°K phonon.

⁴⁴ The notation is due to L. B. Bouchaert, R. Smoluchowski, and E. Wigner, Phys. Rev. **50**, 58 (1936), and is used for the group-V semimetals by M. H. Cohen, L. M. Falicov, and S. Golin, IBM J. Res. Develop. **8**, 215 (1964); L. M. Falicov and S. Golin, Phys. Rev. **137**, A871 (1965).

⁴⁵ B. Abeles and S. Meiboom, Phys. Rev. **101**, 544 (1956), especially Table II; see also Ref. 22; R. T. Bate and N. G. Einspruch, Phys. Rev. **153**, 796 (1967). These authors rule out the possibility of another band, but in their Fig. 4 the band models overestimate the data. Presumably the presence of another band would slow the rate of change of the extremal areas with doping. See also Ref. 6.

C. Impurity Scattering

A quantitative analysis of the effect of impurities upon the recombination is not possible since neither the exact nature nor the amount of impurities present in our samples could be determined. A criterion for the sample purity is the ratio of resistivities at 300 and 4.2°K. Measurements^{20,21} at low temperatures show $\rho(T) \propto T^2$, leveling off typically below 4°K to a value ρ_I roughly proportional to N_I , the impurity density.⁴⁶ For sample 2, among the purest samples reported,^{20,47} the intrinsic mechanisms for electrical conductivity remain dominant even at 4.2°K (see Fig. 11), making a meaningful estimate of the relative N_I in our samples possible only from data for $T \leq 2^\circ\text{K}$. From Fig. 11,

$$\rho_I(1)/\rho_I(2) \approx N_I(1)/N_I(2) \approx 2.5 \quad (30)$$

and from Eq. (27),

$$\tau_I^{-1}(1)/\tau_I^{-1}(2) \approx 2. \quad (31)$$

This supports the idea that the impurity scattering contribution to the electron-hole recombination in bismuth can be characterized by a temperature-independent τ_I such that

$$\tau_I^{-1} \propto N_I. \quad (32)$$

D. Possible Mechanism for Recombination

In addition to the single phonon-aided recombination mechanism, there is the possibility of a double electron-hole pair recombination taking place with energy and crystal momentum being conserved by the four particles. The particular geometry of the Brillouin zone of bismuth allows this. Such a process can be regarded as an electron-electron interaction by which both electrons are scattered to final states in the valence band. Such a process is characterized⁴⁸ by $\tau_{ee}^{-1} \propto (kT/E_F)^2$, a temperature dependence which does not in any way describe our experimental results. Furthermore, the scattering involves large momentum changes for the individual particles; the large dielectric constant of bismuth (~ 100) and the resulting large screening radius makes the process unlikely.

E. Recombination Contribution to Total Carrier Scattering

Using the mass parameters of Galt *et al.*,⁴⁹ Zitter⁵⁰ obtained τ_e and τ_h from measurements on the low-field galvanomagnetic coefficients at 4.2°K:

$$\tau_e \approx 2 \times 10^{-10} \text{ sec}, \quad \tau_h \approx 4.5 \times 10^{-10} \text{ sec}, \quad (33)$$

⁴⁶ R. N. Bhargava, *Phys. Rev.* **156**, 785 (1967).

⁴⁷ P. Cucka and C. S. Barrett, *Acta Cryst.* **15**, 865 (1962).

⁴⁸ For example, D. Pines, *Elementary Excitations in Solids* (W. A. Benjamin, Inc., New York, 1963), p. 276; E. Abrahams, *Phys. Rev.* **95**, 839 (1954); M. J. Katz, S. H. Koenig, and A. A. Lopez, *Phys. Rev. Letters* **15**, 828 (1965); W. G. Barber, *Proc. Roy. Soc. (London)* **A158**, 383 (1937); N. F. Mott, *Advan. Phys.* **13**, 325 (1964).

⁴⁹ J. K. Galt, W. A. Yager, F. R. Merritt, B. B. Cetlin, and A. D. Brailsford, *Phys. Rev.* **114**, 1396 (1959).

where τ_e and τ_h represent a typical component of the diagonalized, nearly isotropic relaxation-time tensor for electrons and holes, respectively.

Since these values were obtained for a sample with a residual resistance ratio ≈ 150 , we would expect the ratio to be approximately two and three times longer for our samples 1 and 2, respectively, judging from the temperature dependence of the resistivity (Fig. 11). Our measured values of τ_R would thus represent a 5–10% contribution from the electron-hole recombination to the total carrier scattering rate at 4.2°K.

From Figs. 11, 12, and Eq. (33), we see that when T is increased to $\sim 15^\circ\text{K}$, τ_R approximately equals the characteristic conductivity relaxation time $\tau_c \sim \tau_e \sim \tau_h$. A 50% contribution from the recombination to the resistivity should then be expected; that is, at $\sim 15^\circ\text{K}$ the carriers will on the average undergo one collision before recombining. The recombination scattering should dominate the resistivity above 20°K, and at 50°K one has $\tau_e \approx 20\tau_R$. This conclusion is self-contradicting, unless the electron-hole recombination does not contribute to loss of the average velocity of the carrier distribution (i.e., the current). We propose the following possible resolution of the paradox.

If the mean free path of the phonons that are emitted in an electron-hole recombination is determined by the lifetime for creating another electron-hole pair, then (somewhat akin to superconductivity) the interaction will not affect the drift velocity of the combined distribution. Rather, the tightly coupled electron-hole-phonon complex will drift until some other scattering event, presumably the phonon-phonon interaction, takes place. This explanation predicts a large phonon drag contribution to, for example, the Nernst coefficient for $T \lesssim 50^\circ\text{K}$, something that can be checked.

One may very crudely estimate whether the phonon mean free path is long enough for this mechanism to be allowed in bismuth. We must estimate and compare the phonon-electron (or hole) and phonon-phonon scattering times, τ_{pe} and τ_{pp} , respectively. From measurements of the heat capacity⁵⁰ and thermal conductivity⁵¹ at 50°K we obtain

$$\tau_{pp} \sim 1.5 \times 10^{-11} \text{ sec}, \quad (34)$$

using a phonon velocity v_p of 10^5 cm/sec. If we allow for a 10% uncertainty width in the phonon momentum (a typical value, judging from linewidths of higher-momentum phonons observed in neutron scattering), then the number of phonons at X or L (case 1 or 2, respectively) that can contribute to recombination for $T \approx 50^\circ\text{K}$ is $\sim 3 \times 10^{20}/\text{cm}^2$, assuming that at this temperature no optical phonons are excited (see Figs. 15 and 16). From Eq. (27) it follows that the 130°K phonon is the dominant one in recombination. Therefore

⁵⁰ N. E. Phillips, *Phys. Rev.* **118**, 644 (1960).

⁵¹ *Natl. Bur. Std. (U. S.) Circ. No. 556*, p. 36; G. K. White and S. B. Woods, *Phil. Mag.* **3**, 342 (1958).

at 50°K

$$N_p(T_p=130^\circ\text{K}) \leq \frac{2}{3} \times (1/13) \times 3 \times 10^{20},$$

since the population probability for such a phonon is 1/13 at 50°K and it represents $\frac{2}{3}$ of the available phonons. The number of carriers^{20,21} n at 50°K is $n = n_e + n_h \approx 7 \times 10^{17}$. τ_{pe} follows from $N_p \tau_{pe} = n \tau_{pe}$:

$$\tau_{pe} \leq \frac{7 \times 10^{-12}}{7 \times 10^{17}} \times 1 \times 10^{19} \approx 10^{-10} \text{ sec.} \quad (35)$$

From Eqs. (34) and (35),

$$\tau_{pe}/\tau_{pp} \leq 7.$$

This very rough estimate of the strength of the interaction of carriers and phonons at X allows for the conjectured mechanism. At temperatures below 50°K, phonons at X drift with the carrier distribution when current is flowing, so that the recombination process does not contribute to the resistivity.

F. Anisotropy of E_{AME}

All anisotropy of the E_{AME} field as given by Eq. (14) is contained in the $\mu_{\text{eff}}H$ factor. Although the carrier mobilities in bismuth are highly anisotropic,³⁰ a fairly isotropic E_{AME} is expected for our experimental arrangement since, as pointed out earlier, $\mu_{\text{eff}} \approx \nu_3$ for H in the trigonal plane. By rotating the magnetic field in the trigonal plane the angular dependence of E_{AME} shown in Fig. 9 is obtained; the anisotropy of E_{AME} is small, as expected.

The electronic structure of bismuth³ consists of three electron ellipsoids located at the L points (see Fig. 1), tilted out of the trigonal plane $\sim +6.5^\circ$,^{2,52} and one hole ellipsoid now known to be at points T . The mobility tensor for electrons at one extremum in the coordinate system with axes 1, 2, and 3 corresponding to the binary,

$$\mu_{\text{eff}}^{-1}(\theta) = \frac{1}{3} \frac{\mu_1 \cos^2\theta + \mu_2 \sin^2\theta}{(\mu_2\mu_3 - \mu_4^2)\sin^2\theta + \mu_1\mu_3 \cos^2\theta} + \frac{2}{3} \frac{(\mu_1 + 3\mu_2)\cos^2\theta + (3\mu_1 + \mu_2)\sin^2\theta \pm 2\sqrt{3}(\mu_2 - \mu_1)\sin\theta \cos\theta}{\{[(3\mu_2 + \mu_1)\mu_3 - 3\mu_4^2]\cos^2\theta + [(\mu_2 + 3\mu_1)\mu_3 - \mu_4^2]\sin^2\theta \pm 2\sqrt{3}[\mu_3(\mu_2 - \mu_1) - \mu_4^2]\sin\theta \cos\theta\}} + 1/\nu_3. \quad (38)$$

Relative magnitudes of $\mu_{\text{eff}}(\theta)$ for E_{AME} parallel to the binary or E_{AME} parallel to the bisectrix axes are obtained by multiplying Eq. (38) by $\cos\theta$ and $\sin\theta$, respectively. The result is shown in dotted lines in Fig. 9. Relative numerical values for the mobility components were obtained by adjusting the measured values of μ_2 , μ_4 , and ν_3 given in Ref. 30 to fit the ex-

⁵² Some confusion exists in the literature as to the sign of the tilt angle. This has been recently clarified by R. D. Brown, III, R. L. Hartman, and S. H. Koenig Phys. Rev. 172, 598 (1968). These authors further show that $\mu_4 < 0$ for a positive tilt angle.

bisectrix, and trigonal directions, respectively, may be written as

$$\mathbf{u} = \begin{pmatrix} \mu_1 & 0 & 0 \\ 0 & \mu_2 & \mu_4 \\ 0 & \mu_4 & \mu_3 \end{pmatrix},$$

where for Bi, μ_4 is a negative quantity.⁵² The mobility tensor for holes is

$$\mathbf{v} = \begin{pmatrix} \nu_1 & 0 & 0 \\ 0 & \nu_1 & 0 \\ 0 & 0 & \nu_3 \end{pmatrix}.$$

The μ_{eff} in Eq. (14) is derived from the S_{ii} component of the conductivity tensor \mathbf{S} , where the E_{AME} is in the i th direction and \mathbf{S} is defined by

$$i_i = \sum_k s_{ik}(\mathbf{H})E_k \quad (36)$$

in the notation of Abeles and Meiboom.⁴⁵ Following a procedure described by these authors, the contributions from the four extrema to the total current may be added to give the total current

$$I_i = \sum_k S_{ik}(\mathbf{H})E_k. \quad (37)$$

Here the lower-case i_i and s_{ik} refer to one ellipsoid, and the upper-case letters represent the sum of all electron and hole band extrema.

In our case $\mathbf{H} = (H \sin\theta, H \cos\theta, 0)$, where θ is the angle between \mathbf{H} and the bisectrix axis. When the magnetic field is rotated about the trigonal axis, $\mu_{\text{eff}}(\theta)$ is obtained from the S_{11} component of the tensor $\mathbf{RS}(H)\mathbf{R}^{-1}$, where

$$\mathbf{R} = \begin{pmatrix} \cos\theta & -\sin\theta & 0 \\ \sin\theta & \cos\theta & 0 \\ 0 & 0 & 1 \end{pmatrix}.$$

The result is

perimental data; the result is

$$\begin{aligned} \mu_2/\mu_1 &= 7 \times 10^{-3}, \\ \mu_3/\mu_1 &= 0.7, \\ \mu_4/\mu_1 &= -8.2 \times 10^{-2}, \\ \nu_3/\mu_1 &= 2.3 \times 10^{-2}. \end{aligned} \quad (39)$$

The major differences between these mobility ratios and those given by Zitter³⁰ are in μ_2/μ_1 and the sign in μ_4/μ_1 .⁵² When \mathbf{H} is along a principal axis, Eq. (38)

TABLE III. Effective ambipolar mobility responsible for the AME field. Numerical values are calculated using Eq. (38).

E_{AME}	H	μ_{eff}^{-1}	$(\text{cm}^2/\text{V sec})$
Binary	Bisectrix	$\frac{1}{3} \frac{1}{\mu_3} + \frac{2}{3} \frac{\mu_1 + 3\mu_2}{(\mu_1 + 3\mu_2)\mu_3 - 3\mu_4^2} + \frac{1}{\nu_3}$	0.94×10^6
Bisectrix	Binary	$\frac{1}{3} \frac{\mu_2}{\mu_2\mu_3 - \mu_4^2} + \frac{2}{3} \frac{3\mu_1 + \mu_2}{\mu_3(3\mu_1 + \mu_2) - \mu_4^2} + \frac{1}{\nu_3}$	1.0×10^6

simplifies considerably, yielding the results shown in Table III, in agreement with Yamada's results.^{19,53}

VI. QUANTUM EFFECTS

The linear dependence of the AME effect on the magnetic field predicted in Eq. (14) is only true in the absence of Landau quantization of the carrier orbits. Experimentally, oscillations similar to de Haas-van Alphen (dHvA) oscillations are observed for $H \geq 1$ kG, and become more pronounced as T is lowered. A typical trace of E_{AME} versus magnetic field is shown in Fig. 17, in which periods of $7.2 \times 10^{-5} \text{ G}^{-1}$, corresponding to the well-established electron periods when the field is parallel to the binary direction, are observed. By rotating the magnetic field in the trigonal plane all electron periods in the plane could be identified except for the very short periods occurring $\pm 3^\circ$ from the binary. The data are shown in Fig. 18, compared to the most recent dHvA results indicated by the dashed line.⁴⁶ No hole periods were observed, because of the limited range of magnetic fields available in the present experiments.

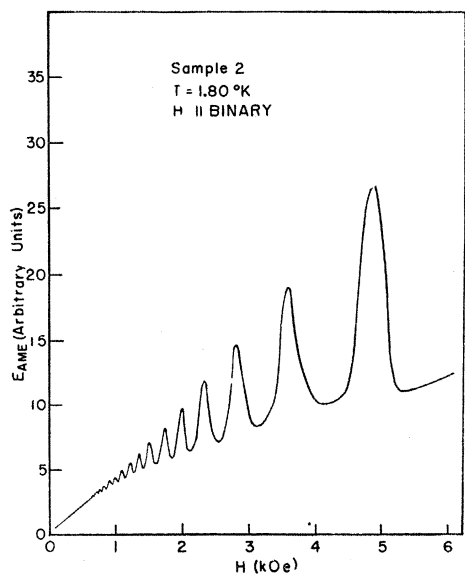


FIG. 17. Actual X-Y recorder trace of E_{AME} versus magnetic field, under optimum experimental conditions for observing quantum effects. The oscillations correspond to electron periods of $7.2 \times 10^{-5} \text{ G}^{-1}$.

⁵³ T. Yamada, J. Phys. Soc. Japan 20, 1966 (E) (1965).

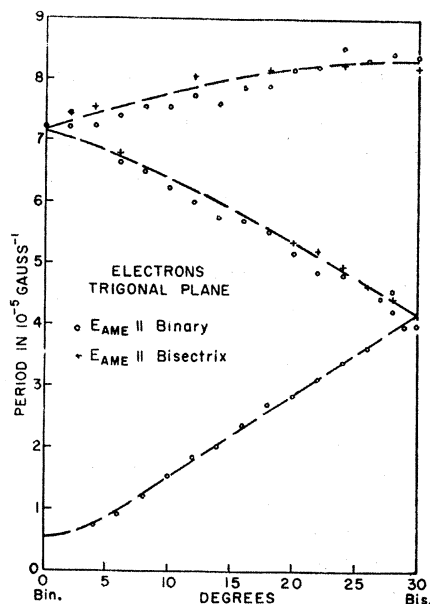


FIG. 18. Electron periods in the trigonal plane, obtained by rotating H in this plane. The dotted line are the dHvA periods given in Ref. 46.

It has been shown in Sec. II that the AME field is proportional to the electronic part of the acoustic attenuation, which in turn is proportional to the excess carrier concentration δn . Therefore the peaks of E_{AME} shown in Fig. 17 are to be associated with the quantized levels crossing the Fermi surface, and correspond to peaks in the total attenuation. The latter is plotted versus field in Fig. 19. Also shown is E_{AME}/H , corrected for attenuation, using $E_{AME}(H)$ from Fig. 17. The

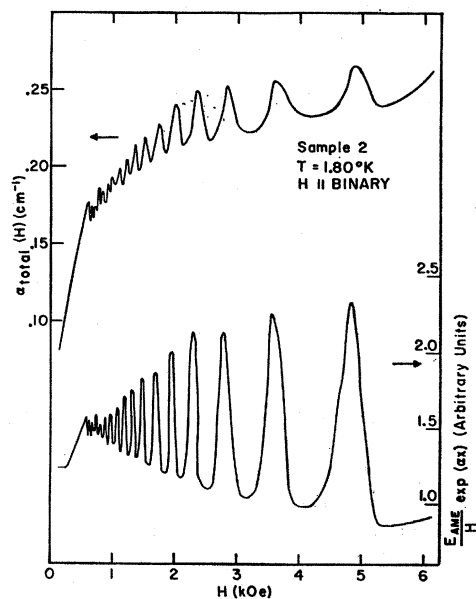


FIG. 19. Upper curve shows the magnetic-field dependence of the acoustic attenuation. Lower trace is a plot of Eqs. (3) and (4) combined, i.e., the magnetic field dependence of α_e . The similarity of both curves and with Fig. 17 is apparent.

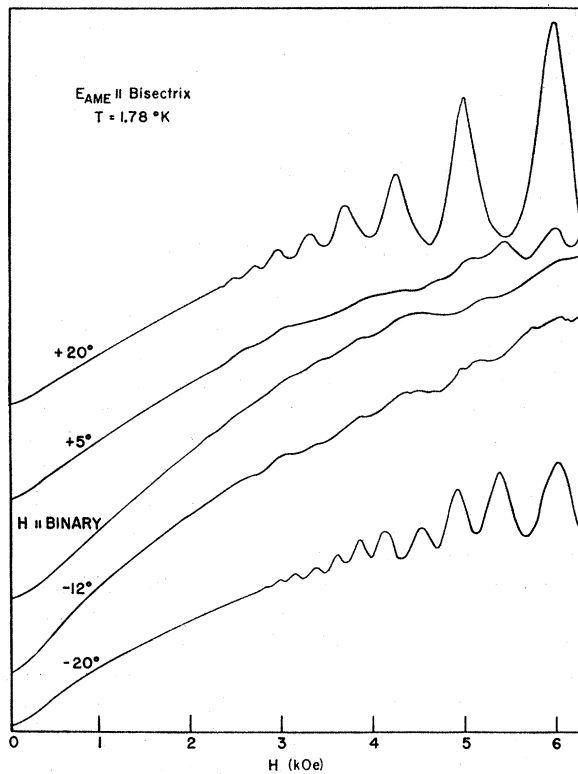


FIG. 20. Fading out of the electron dHvA-like periods when the magnetic field is rotated through the binary direction. $\mathbf{H} \parallel \text{binary}$ corresponds to an angle of 0° .

similarity of the two quantities is apparent, as predicted by Eqs. (3) and (4).

Yamada¹⁹ has shown in detail that the amplitude of the oscillations is as expected from the magnetic-field dependence of the density of states, assuming the appropriate values for the Fermi energy and carrier effective masses.

When \mathbf{H} was rotated into a particular binary direction, the oscillations for $\mathbf{E}_{\text{AME}} \parallel \text{bisectrix}$ faded out, as is shown in Fig. 20. The detailed analysis of the dHvA effect⁵⁴ shows that the amplitude of the oscillations is proportional to $e^{-1/HP}$, where H is the magnetic field in Gauss and P is the period in G^{-1} . For the amplitude of the oscillations to remain constant requires that HP remain constant. Therefore, since P decreases at fixed H as \mathbf{H} approaches the binary direction (see Fig. 20), the amplitude decreases. This presumably is also the explanation for Yamada's observation (see Fig. 11 of Ref. 19).

The magnetic-field dependence of the attenuation coefficient $\alpha(H)$ in the magnetic-field range reported here has been previously investigated by Toxen and Tansal.²² They interpreted their data on the basis of a "giant-oscillation" mechanism first proposed by

⁵⁴ I. M. Lifshitz and A. M. Kosevich, Zh. Eksperim. i Teor. Fiz. **29**, 730 (1955) [English transl.: Soviet Phys.—JETP **2**, 636 (1956)].

Gurevich *et al.*⁵⁵ This interpretation has recently been questioned by Mase *et al.*⁵⁶ Our interpretation of α , based on the interaction of the classical sound field with the carriers via the deformation potential, yields quantitative agreement with all the present experimental results, in both the quantum and nonquantum limits. It also predicts that any oscillations in $\alpha(H)$ should be of the dHvA type, arising from the magnetic-field-dependent carrier density of states. In fact, all the observed oscillations in χ could be identified with the known⁴⁶ electron dHvA periods in the trigonal plane (cf. Fig. 18).

VII. SUMMARY

We have shown that the emission and absorption of phonons of energies $43 \pm 4^\circ\text{K}$ and $130 \pm 15^\circ\text{K}$ constitute the main mechanism for electron-hole recombination in bismuth, mitigated at low temperatures by a temperature-independent impurity scattering.

From first-order perturbation theory, assuming emission or absorption of a single phonon with energy conservation, we showed that a single recombination time τ_R could be defined, and derived the theoretical temperature dependence of τ_R . It was by comparison of the data with the theory that the above phonon energies were obtained. A comparison was made with the recently completed data for the phonon-dispersion curves in an attempt to determine unequivocally whether the maximum of the hole band is at T or Γ . Our two activation energies agree very well with phonon energies at X , indicating that the hole band is located at T . The possible existence of another hole band at Γ cannot however be ruled out; our 130°K phonon agrees with optical phonon energies at L as well as X . In any case this band, if present, must have its maximum about 10 meV (the energy associated with 130°K) below the Fermi surface, since no contributions from it are apparent at low temperatures.

Using the best, but by no means certain, theoretical results for the symmetry of the conduction- and valence-band wave functions, we have shown that one acoustic and two optical phonons are allowed by symmetry to couple the electron and hole bands, whether the holes are at T or Γ . The phonon-selection rules are consistent with the holes being located at T , and support our conclusion that any hole-band maximum at Γ must be below the Fermi surface, since the acoustic phonon allowed at L is not observed in the present experiments.⁵⁷

Mase's conduction-band labeling could not be unequivocally verified since wave functions of either even

⁵⁵ V. L. Gurevich, V. G. Skobov, Y. A. Firsov, Zh. Eksperim. i Teor. Fiz. **40**, 786 (1961) [English transl.: Soviet Phys.—JETP **13**, 552 (1961)].

⁵⁶ S. Mase, Y. Fujimori, and H. Mori, J. Phys. Soc. Japan **21**, 1744 (1966).

⁵⁷ A summary comparing the neutron data, the AME data, and the group-theoretical results has been published: S. H. Koenig, A. A. Lopez, D. B. Smith, and J. L. Yarnell, Phys. Rev. Letters **20**, 48 (1968).

or odd character yield selection rules compatible with our results. We believe, however, that Mase's labeling, namely, L_6+L_6 (C_3+C_4 in Mase's notation, odd under inversion), is probably correct, since it allows a greater number of $\sim 130^\circ\text{K}$ phonons than 43°K phonons, and the data show that the total matrix element for the interaction with the 130°K phonons is greater than with the 43°K phonon [Eq. (27); $B \gg A$].

The relation between τ_R and the AME effect as given by Eq. (14) was examined in detail. The frequency dependence was verified, and in fact used to normalize the results τ_R . From the magnitude of E_{AME} and an estimate of the sonic energy flux an estimate of the deformation potential ($|E_1 - E_2| \geq 1.5$ eV) is obtained that is consistent with the known value.²³ The anisotropy of the E_{AME} is explained in terms of the low field mobility anisotropy. The linear magnetic-field dependence was verified for fields below those for which quantum effects are significant. At higher values of magnetic field, quantum oscillations are observed in E_{AME} . The oscillations are interpreted as resulting from the dependence of the ultrasonic attenuation coefficient α on the magnetic-field-dependent density of states at the Fermi surface, much in the manner of the dHvA effect. The angular dependence of the period of the oscillations is in excellent agreement with the most recent dHvA results.⁴⁶

We have shown that an important contribution to the ultrasonic attenuation in bismuth at low temperatures is that associated with the repopulation of the energy bands induced by the ultrasonic strain, via the deformation-potential interaction. This effect, described by Keyes, is the dominant attenuation mechanism below $\sim 20^\circ\text{K}$ for the range of frequency and magnetic field used here.

Finally, we show that above $\sim 20^\circ\text{K}$ the measured recombination time is shorter than the conductivity

relaxation time; at 50°K , $\tau_c \approx 20\tau_R$. A resolution of this paradox can only be had if the phonons are so highly coupled to the carriers via this interaction that they drift with them. This predicts a large phonon-drag⁵⁸ contribution to the thermoelectric power in the temperature range $\leq 50^\circ\text{K}$, which should be investigated.

ACKNOWLEDGMENTS

The author would like to thank Professor George Busch of the Swiss Federal Polytechnic Institute (ETH), Zurich, for sponsorship of this work in partial fulfillment of the requirement for the degree of Doctor of Philosophy; Dr. Seymour H. Koenig for suggesting the present investigation, for his continued guidance (particularly in obtaining the phonon-selection rules), and for his encouragement throughout the work; Dr. Robert L. Hartman, who supplied the crystals, and with whom, together with Dr. Rameshwar N. Bhargava, Rodney D. Brown, Jose Fortoul, and Walter Schillinger, stimulating discussions were enjoyed; Dr. Peter J. Price for several helpful conversations; Dr. Darryl Smith for making his phonon data available prior to publication and for several discussions and suggestions regarding the phonon labelings; Professor J. Birman for an introductory discussion in the methods of group theory; Mrs. Alice Kelbl for the drawings, and other members of the IBM Watson Laboratory staff who made the stay such a pleasant one. The author is grateful to Professor Golin (University of Pittsburgh) for making his paper available prior to publication, and to Professor Pratt (MIT) for making the author aware of Dr. Ferreira's papers prior to publication.

⁵⁸ See J. M. Ziman, *Principles of the Theory of Solids* (Cambridge University Press, Cambridge, England, 1964), p. 209.

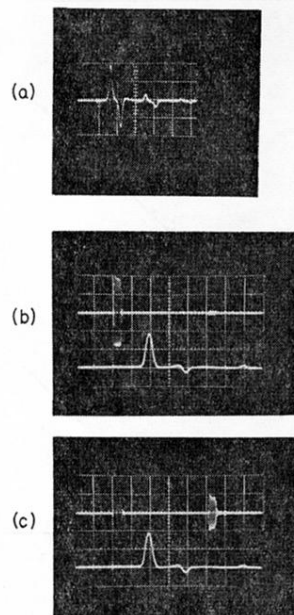


FIG. 3. (a) Pulse waveform of E_{AME} in sample 1. Horizontal scale = $10 \mu\text{sec}$ /large division. Trace shows several double passages of the sonic pulse past the electrodes. Rf pickup can barely be seen at $\sim 6 \mu\text{sec}$ before first E_{AME} pulse. The rf frequency used was 11 MHz. (b) Upper trace: rf main pulse. Vertical scale = 10 V /large division, horizontal scale = $10 \mu\text{sec}$ /large division. First reflected echo at $\sim 50 \mu\text{sec}$ delay. Lower trace: E_{AME} pulse waveform in sample 2. Peak of the pulse occurs at a time lag corresponding to a distance of $\sim 3 \text{ cm}$ from the transducer end of the sample, measured from the center of rf pulse. (The rf frequency was 6.2 MHz.) (c) Same as (b) but vertical scale on upper trace = 1 V /large division to show first rf echo. $H = 5.0 \text{ kOe}$ and \parallel bisectrix for (a)-(c).